Structural Engineering and Mechanics, Vol. 37, No. 2 (2011) 131-147
DOI: http://dx.doi.org/10.12989/sem.2011.37.2.131

Application of joint time-frequency distribution for estimation of time-varying modal damping ratio

H. Bucher, C. Magluta and W.J. Mansur*

Department of Civil Engineering, COPPE/Federal University of Rio de Janeiro, CP 68506, CEP 21945-970, Rio de Janeiro, RJ, Brazil

(Received March 4, 2009, Accepted May 10, 2010)

Abstract. The logarithmic decrement method has been long used to estimate damping ratios in systems with only one modal component such as linear single degree of freedom (SDOF) mechanical systems. This paper presents an application of a methodology that uses joint time-frequency distribution (JTFD) as input, instead of the raw signal, to systems with several vibration modes. A most important feature of the present approach is that it can be applied to a system with time-varying damping ratio. Initially the precision and robustness of the method is determined using a synthetic model with multiple harmonic components, one of them displaying a time-varying damping ratio, subsequently the results obtained from experiments with a reduced model are presented. A comparison is made between the results obtained with this methodology and those using the classical technique of Least Squares Complex Exponential Method (LSCE) in order to highlight the advantages of the former, such as, good precision, robustness and excellent performance in extreme cases, e.g., when very low frequency components and time varying damping ratio are present.

Keywords: damping; modal damping; joint time-frequency distribution (JTFD); least squares complex exponential method (LSCE).

1. Introduction

Characterization of the damping properties of mechanical systems is greatly simplified when only one frequency component is present in the signal, and the damping ratio can be clearly estimated through the method of logarithmic decrement (Thomson 1998, Rao 1995, Clough and Penzien 1993, Weaver and Jonhnston 1987, Meirovich 1986, Paz and Leigh 2003).

This task becomes complex when there are several frequency components, corresponding to distinct vibration modes, and the use of more sophisticated methods (Staszewski 1997, 1998, Boltežar and Slavič 2002, Lamarque *et al.* 2000, Kareem and Gurley 1996, Bucher 2001, Ibrahim and Mickulcik 1977, Bodeux and Golinval 2003, Zhang *et al*. 2005, Mohanty and Rixen 2006, Wang and Liu 2010, Katkhuda *et al.* 2010, Nagarajaiah and Basu 2009) to characterize the mechanical system loss of energy is necessary. Many of the existing techniques are based on the fact that the structure behavior is linear and the damping ratio does not vary, limitations unacceptable in many current engineering design works.

*Corresponding author, Ph.D., E-mail: webe@coc.ufrj.br

Wavelets (Burrus *et al.* 1998, Carmona *et al.* 1997, Daubechies 1992, 1996, Mallat 1999, Rioul and Duhamel 1992, Todorovska 2001, Morlet *et al.* 1982, Kijewski and Kareem 2002a, b, Gökda and Kopmaz 2010) and other time-frequency distributions (TFD) (Roshan-Ghias *et al.* 2007, Bucher 2001, Ville 1946, Wigner 1932, Wigner 1971, Cohen 1966a, b, 1995, 1996, Choi and Williams 1989, Zhao *et al.* 1990, Atlas *et al.* 1992, Cunningham *et al.* 1993, Cunningham and Williams 1996) have been intensively employed for the identification of different characteristic of mechanical systems, e.g., damping ratio (Staszewski 1997, 1998, Boltežar and Slavič 2002, Lamarque *et al.* 2000, Kareem and Gurley 1996, Bucher 2002), damage (Boulahbal *et al.* 1999, Lin and Qu 2000, Staszewski and Tomlinson 1994), wind loads (and other natural phenomena) (Gurley and Kareem 1999, Kareem and Kijewski 2002), and see also (Farge 1992, Piombo *et al.* 2000, Gurley *et al.* 2003, Kijewski and Kareem 2003) for other applications. The choice of the most adequate technique depends strongly on which characteristics of the mechanical system are under study. In this paper a time-frequency distribution (TFD) is employed for the determination of damping characteristics of structural systems; the new methodology discussed here showed to be quite reliable.

Joint time-frequency distribution (JTFD) transforms a signal time-sampling into a distribution in the time-frequency space, thus making possible to analyze individually the components corresponding to the natural frequencies. JTFD permits decomposing a time-response signal of a structural system into its modal components, so that the damping ratio of each modal component can be estimated through a modified form of the method of the logarithmic decrement. As the method permits the identification of the time variation of the amplitude component of each mode, it is possible to characterize variable damping ratios. In order to characterize the variation of modal damping ratio with amplitude a new variable is introduced, the normalized amplitude v, obtained from the JTFD, whose time derivative is defined as the damping ratio. From the normalized amplitude versus time curve the damping ratio, which is the slope of this curve, can be determined using statistical methods (as a linear regression). The use of statistical methods is the major factor of robustness of the method presented here since it provides means to obtain directly not only the damping ratio value, but also a measure of its error through the correlation value.

The main objective of the present paper is to show the application of a robust and versatile methodology based on a JTFD, which allows analyzing structures whose damping ratio is not invariant. The methodology described here permits visualizing whether or not the damping ratio varies over time; and when it does, it is possible to have good piecewise damping ratio estimates. The length of validity of the time interval in such a piecewise estimation can be easily inferred from the modal amplitude versus time curves.

The variation of the damping ratio of structures is usually associated to the displacement amplitude, as in the case of flexible risers (especial tubes used in the offshore industry) (Magluta *et al.* 2001) or in some offshore platforms. In this paper only free vibration response signals are analyzed, thus the displacement amplitude decays with time. In fact, damping ratio may depend on time-varying variables, such as displacement amplitude; however, to simplify notation, damping ratio is indicated just as a time-dependent variable.

The present paper also shows that the results obtained for the same time intervals using a classical technique, such as the Least Squares Complex Exponential method (LSCE) (Allemang and Brown 1987), are quite close to those obtained with the method presented here. Two great advantages of the methodology described here to compute damping ratio are that: (a) it permits a clear identification of the variation profile of the damping ratio with time; (b) it permits computing average values in short time intervals leading to a better understanding of the real damping characteristics of the mechanical system.

The versatility and other important features of the present methodology are shown through two examples: a synthetic one and an experimental one. These examples confirm the great potential of this methodology to identify damping characteristic of structures.

2. Damping models

The kinetic time-response amplitude of a SDOF mechanical system in harmonic motion, with angular frequency Ω (rad/s), may be written in the following general form

$$x(t) = \rho(t)e^{i(\Omega t + \theta)} \tag{1}$$

in which $x(t)$ is a complex variable whose real part describes the instantaneous position of the body, $\rho(t)$ is the instantaneous amplitude of the mass displacement and θ is a phase constant dependent of initial conditions. The total energy, kinetic plus potential, of such system is proportional to the square of the instantaneous amplitude (Peters 2005)

$$E(t) = B\rho^2(t) \tag{2}$$

where, B is constant dependent of mass and stifness of the system (see Rao 1995).

The damping, and consequently the loss of energy, can be quantified through the viscous damping ratio ξ, which may be related to the logarithmic decrement δ (Thomson 1998, Rao 1995, Clough and Penzien 1993, Weaver and Jonhnston 1987, Meirovich 1986, Paz and Leigh 2003). Both may be directly written as a function of the total energy loss ΔE per cycle as

$$\xi = \frac{\delta}{2\pi} = -\frac{1}{4}\frac{\Delta E}{E(t)} = -\frac{1}{4\pi}\frac{E(t+T) - E(t)}{E(t)} \tag{3}$$

where $E(t)$ is related to a component (mode) at the beginning of the cycle and T is its period. Eq. (3) describes the classical way to quantify damping. The procedure employed here permits quantifying damping through the instantaneous damping ration $\xi(t)$ given by

$$\xi(t) = -\frac{1}{2\Omega}\frac{\partial E(t)/\partial t}{E(t)} \tag{4}$$

and using the expression of the derivative of the natural logarithm, the following equation is obtained

$$\xi(t) = -\frac{1}{2\Omega}\frac{\partial}{\partial t}\log E(t) \tag{5}$$

This last equation is the key for the present analysis as it expresses damping as a continuous function of the instantaneous loss of energy of the system. Therefore the new variable $\xi(t)$ is named instantaneous damping ratio.

In this work the viscous damping model is used as the starting point but most other damping models may be used within this framework as well. Hysteretic damping ratio, for example, may be directly related, for low damping ratios, to the viscous damping ratio through the following equation (Rao 1995).

$$\delta = \pi\beta = 2\pi\xi \tag{6}$$

where β is a constant indicating a dimensionless measure of hysteretic damping. The value of ξ above guarantee that the energy dissipated by an equivalent viscous model is equal that of a hysteretic model at the natural frequency.

3. Joint time-frequency transforms

The general form of time-frequency transforms (Cohen 1995) states that any JTFD $C_f(t, \omega)$ of a complex function $f(t)$ may be rewritten as the Fourier transform of a particular autocorrelation function $R_f(t, \tau)$ such that

$$C_f(t, \omega) = \frac{1}{4\pi^2}\int_{-\infty}^{+\infty} R_f(t, \tau)e^{-i\omega\tau}d\tau \tag{7}$$

where

$$R_f(t, \tau) = \int_{-\infty}^{+\infty} f\left(u + \frac{1}{2}\tau\right)f^*\left(u - \frac{1}{2}\tau\right)\Phi(t-u, \tau)du \tag{8}$$

The function $\Phi(t, \tau)$ that appears in Eq. (8) is called window and is obtained through the Fourier transform of the kernel of the distribution $\phi(\theta, \tau)$

$$\Phi(t, \tau) = \int_{-\infty}^{+\infty} \phi(\theta, \tau)e^{-it\theta}d\theta \tag{9}$$

Different families of joint time-frequency distributions may be obtained choosing different kernels. Several types of kernels have been already developed, each one with their own particular properties, making them more or less suitable for a particular application.

4. Methodology

By introducing a damping behavior, the harmonic system, see Eq. (1), becomes

$$v(t) = \rho e^{i(\Omega t + \theta)}e^{-\xi\Omega t} \tag{10}$$

where ρ and θ are constants dependent of initial conditions, Ω is the mode frequency and ξ is the damping ratio. The energy of such system may be derived from Eq. (11) by using definition (2) so that

$$E_\Omega(t) = \rho^2 e^{-2\xi\Omega t} \tag{11}$$

The present paper proposition considers that the joint time-frequency distribution $C_f(t, \omega)$ of a signal $f(t)$ containing one harmonic vibration component with angular frequency Ω may be related to its instantaneous energy $E = E_\Omega(t)$. This energy related to a given modal frequency is directly proportional to the value of the JTFD in the vicinities of that frequency Ω, i.e., the energy $E = E_\Omega(t)$ may be estimated using the value of $C_f(t, \omega)$ when values of ω are close to Ω. This process can be done using a transfer function $\alpha(\omega, \Omega)$ defined such that

$$C_f(t, \Omega) = \alpha(\omega, \Omega) E_\Omega(t) \tag{12}$$

where $C_f(t, \Omega)$ represent JTFD of the energy $E = E_\Omega(t)$. In practice this transformation is performed, using the Eqs. (7) and (8) and taking only the associated values to the frequency Ω.

This hypothesis is valid only if the time-frequency distribution $C_f(t, \omega)$ considers the energy conservation condition and time/frequency marginal conditions (Cohen 1995).

Substituting Eq. (12) into Eq. (5) leads to (note that the subscript f has been suppressed to simplify notation)

$$\xi_\Omega(t) = -\frac{1}{2\Omega}\frac{\partial}{\partial t}\log(C(t, \Omega)) \tag{13}$$

The joint time-frequency distribution $C_f(t, \omega)$, calculated from the signal f is then directly related to the instantaneous damping ratio $\xi(t)$. It should be observed that the energy transfer function was completely eliminated by the temporal derivative for being constant over time. Eq. (13) may then be rewritten in an analogous form, more suitable to statistical analysis, by defining a new variable called the normalized modal amplitude v which is given by

$$v_\Omega(t) = \frac{\log(C(t, \Omega))}{2\Omega} \tag{14}$$

such that the damping ratio is defined as its slope (negative)

$$\xi_\Omega(t) = -\frac{\partial}{\partial t}v_\Omega(t) \tag{15}$$

If in a stretch of a plot of v_Ω versus time the damping ratio is considered constant then a simple linear regression may be used to calculate ξ as follows

$$\xi_\Omega = -\frac{\Delta v_\Omega}{\Delta t} \tag{16}$$

A standard error propagation procedure gives an upper bound for the error of this estimative as

$$Error(\xi_\Omega) = \xi_\Omega\left(\frac{Error(v_\Omega)}{\Delta v_\Omega} + \frac{Error(t)}{\Delta t}\right) \tag{17}$$

5. JTFD precision

Due to the uncertainty principle, it is impossible that a joint time-frequency distribution offers arbitrary precision on both time and frequency simultaneously, creating a tradeoff situation.

However, it is possible to choose an arbitrary precision in one domain, which will set automatically the precision in the other. This precision is set when the parameters for the kernel/window, Eq. (8), used are defined.

In practice signals are composed by subcomponents in different frequencies but it is possible to set different precisions in time and frequency for each subcomponent being analyzed. The duration of the mode *Dm* is defined as the time period during which the energy of the subcomponent is much higher than the background noise.

The effective width σ of the window function $\Phi(t, \tau)$ is in practice bounded by two empirical values as indicated below:

1 - Low limit: when $\sigma \approx T$, i.e., when precision becomes poor in frequency domain;

2 - Upper limit: when $\sigma \approx Dm$, i.e., when precision becomes poor in time domain.

In the case of the spectrogram, using blackman, gaussian, hamming or hanning windows, the effective width σ of the adopted window may be taken as 1/4 of their nominal width *L*.

These limits may be used to define a time uncertainty η of this particular analysis, in which f is a frequency; thus

$$\frac{T}{\eta} = \frac{1}{\eta f} < \sigma < \eta Dm \tag{18}$$

A time uncertainty of 100% corresponds to a time uncertainty equal to the duration of the signal. As borders usually introduce noise into the transform when calculating the autocorrelation function given by Eq. (8), alternatively the time uncertainty may be interpreted as a contamination factor. Therefore, a 100% time uncertainty factor introduces border effects that affect the whole extension of the signal.

Heuristics indicates that, the greater the time uncertainty, the better the precision in frequency domain and vice versa. For the limit where both low and high limits are exactly the same the value of the time uncertainty is the minimum possible and is given by

$$\eta_{\min} = \sqrt{\frac{1}{fDm}} \tag{19}$$

It is possible to obtain a conservative estimative for the signal duration *Dm* indirectly from the damping ratio ξ, which despite unknown a priori – it is the subject of the study – lower and upper limits for it are widely known for common structures. For such it is necessary to define the amplitude ratio *R*, calculated as the ratio between the maximum modal amplitude $A_{\max}$ and the minimum $A_{\min}$, generally equal to the background noise level

$$R = \frac{A_{\max}}{A_{\min}} \tag{20}$$

which can be rewritten using Eq. (2) as follows

$$R^2 = \frac{E_{\max}}{E_{\min}} \tag{21}$$

Substituting Eq. (21) into Eq. (14)

$$v_0 = \frac{\log(E_{\max})}{2\Omega} = \frac{\log(R^2 E_{\min})}{2\Omega} = \frac{2\log(R)}{2\Omega} + \frac{\log(E_{\min})}{2\Omega} \tag{22}$$

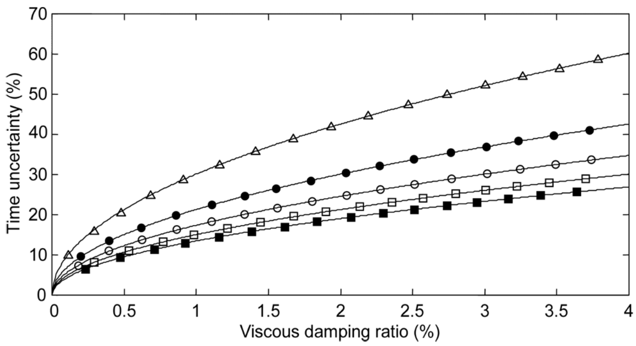

Fig. 1 Minimum contamination levels (or time uncertainties) as a function of the viscous damping ratio for several amplitude ratios. △ - R = 2; ● - R = 4; ○ - R = 8; □ - R = 16; ■ - R = 32

$$v_1 = \frac{\log(E_{\min})}{2\Omega} \tag{23}$$

If the damping ratio is constant Eq. (13) can be written as

$$\xi = -\frac{\partial v}{\partial t} = -\frac{v_1 - v_0}{Dm} = \frac{2\log R}{2\Omega Dm} = \frac{\log R}{2\pi f Dm} \tag{24}$$

and yet, substituting the last result into Eq. (19) it is possible to obtain an estimative for the minimum temporal uncertainty as a function of the maximum damping ratio

$$\eta_{\min} = \sqrt{\frac{2\pi\xi}{\log R}} \tag{25}$$

Fig. 1 shows the minimum temporal uncertainty calculated using the last equation. Note that for high damping ratios it is necessary for the signal component amplitude to be away above the background level (high R values) in order to achieve low uncertainty levels and contamination factors. For a component with an initial amplitude of only twice the background noise ($R = 2$), a damping ratio of 1% would induce a minimum time uncertainty of 30%.

The amplitude ratio R may be obtained directly from the normalized modal amplitude v graph through the equation

$$R = e^{-\Omega \Delta v} \tag{26}$$

In the case of constant damping ratio, after some algebraic operations using Eq. (13) it can be demonstrated that an upper bound for the error on the damping ratio determination may be given by

$$\Delta\xi \leq \frac{\log\left(\dfrac{1+\lambda}{1-\lambda}\right)}{\Omega Dm} \cong \frac{\lambda}{n\pi} \tag{27}$$

where n is the number of cycles present during the duration of the component and λ is the maximum error (dimensionless) in the computation of the distribution $C_f(t, \omega)$. For example, if the maximum error in the distribution is 20% ($\lambda = 0.2$) and the number of cycles is 100 then the maximum error of the computed damping ratio is 0.06%.

6. Synthetic signal

A synthetic signal was created to verify the precision of the described method. A signal

$$v(t) = \sum_{j=1}^{4} A_j e^{-\xi_j \omega_j t} \sin(\omega_j t) \tag{28}$$

was constructed which represents the impulsive response of a single degree of freedom mechanical system; the parameters required by this equation are presented in Table 1, where the parameter A is the signal amplitude, ξ is the damping ratio and ω is the natural frequency.

Note that the component four in Table 1 has a time dependent damping ratio. Fig. 2 shows the synthetic signal amplitude time variation and its frequency spectrum. From the latter the natural frequencies of the response are obtained, in good agreement with the analytical values employed.

To calculate the joint time-frequency distribution (JTFD) to feed Eq. (14), the spectrogram $SP(t, \omega)$ used is given by

$$SP(t, \omega) = \int v(\tau) h(\tau - t) e^{-i\omega\tau} d\tau \tag{29}$$

where $h(t)$ is an arbitrary windowing function, usually the Gaussian $h(t) = e^{-(t/\sigma)^2}$. Then the lines corresponding to the modal frequencies (Ω_j = 10, 25, 40 and 80 Hz) were extracted from the JTFD,

Table 1 Parameters for creation of the synthetic signal

Component	Frequency (Hz)	Damping ratio (%)	Amplitude
1	10	0.10	5
2	25	0.20	81
3	40	0.30	140
4	80	0.10 + 0.95 t	8500

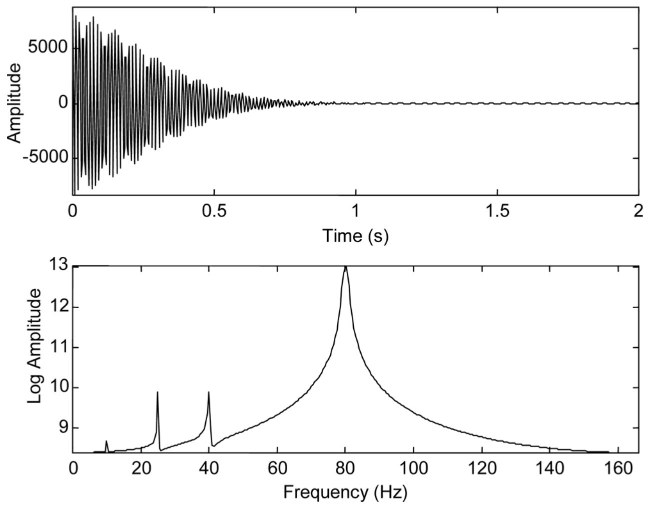

Fig. 2 Synthetic signal and corresponding Fourier transform

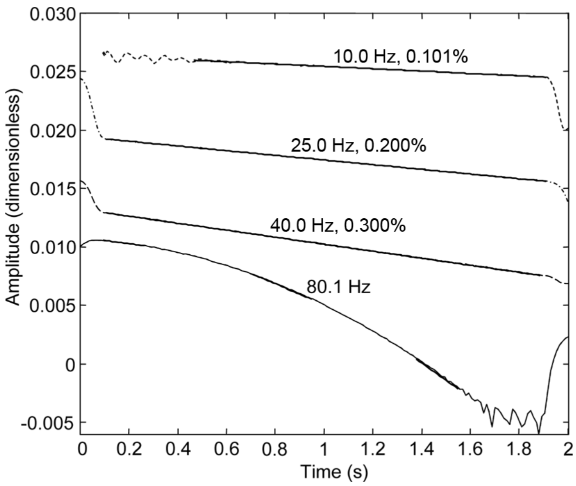

Fig. 3 Normalized amplitude versus time for the synthetic signal described by Eq. (28) with components 10 Hz, 25 Hz, 40 Hz and 80 Hz as shown in Table 1. Percentual values of numerical and analytical (see Table 1) damping ratios coincide up to the third figure

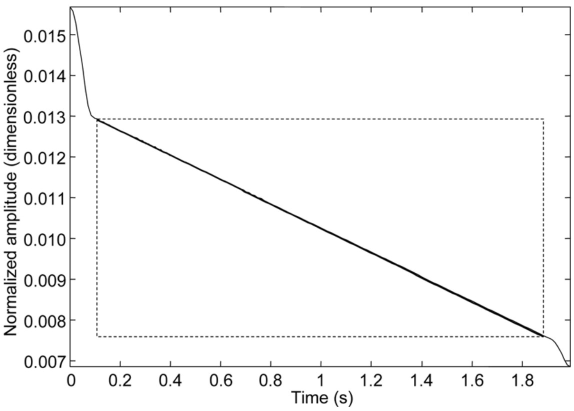

Fig. 4 Normalized amplitude versus time for the synthetic signal for the third component (40 Hz). JTFD computed damping ratio is ξ = (8.0129 – 0.0076)/(1.8821 – 0.1070) = 0.301%

which produced four functions $C_f(t,\Omega)$ for j = 1, 2, 3 and 4. Each function was then used to plot and calculate its respective normalized amplitude $v_\Omega(t)$ using Eq. (14) as seen in Fig. 3, which presents the four normalized amplitude curves of the synthetic signal.

A stretch of the third component (40 Hz) shown in Fig. 4 was selected for linear regression as indicated. The line best fitting is shown as a thick line in Fig. 4 and its bounds are indicated by a dotted box. Its bounds were then used to calculate the damping ratio, as shown by the equation indicated in the caption of this figure, with an estimate of (0.301% ± 0.003%). Eq. (17) was used to calculate the error of the estimate, assuming an error of 0.0001 for the normalized amplitude v and 0.01 s for the time measurement.

Computations of the damping ratios as indicated before produced as expected, constant damping ratios for the first, second and third constant components, the values found being quite close to those used to generate $v(t)$ as indicated by Eq. (28). On the other hand, Fig. 3 shows that the curve dimensionless amplitude versus time for the fourth signal component is non-linear, as expected, as the corresponding damping ratio varies linearly with time. Table 2 presents the expected results and those obtained for this fourth component for five time intervals. It is important to highlight that the expected values for the fourth component were obtained computing the average of the damping ratios at the beginning and the end of the considered time interval as indicated by the Eq. (30), where t_{ini} and t_{fin} are the initial time and final time, respectively. In the same table, results obtained using Least Squares Complex Exponential method (LSCE) (Allemang and Brown 1987) are also presented.

$$\xi = \frac{(0.10 + 0.95t_{ini}) + (0.10 + 0.95t_{fin})}{2} \tag{30}$$

Table 2 shows that the values obtained by JTFD are quite close to those of LSCE method as well as to the expected values, even when a long time interval is considered (0-12 s). This indicates

Table 2 Comparison between expected and estimated damping ratio (%) obtained through the JFTD and LSCE methods for the synthetic signal fourth component

Time interval (s)	Expected (%)	JTFD (%)	LSCE (%)
0.0-0.2	0.20	0.20	0.19
0.2-0.4	0.39	0.40	0.38
0.4-0.6	0.58	0.59	0.58
0.6-1.2	0.96	0.96	0.92
0.0-1.2	0.67	0.68	0.64

clearly that the LSCE result is an average value for the damping ratio which is close to that computed using JTFD and Eq. (30). The great advantage of the latter is that it permits a clear identification of the variation of the damping ratios (and normalized amplitude) with time, and also permits visualizing and computing average values in small time intervals, leading to better understanding of the real characteristics of the mechanical system.

This process may be refined so that the whole signal duration is divided into small line stretches, which can then be individually submitted to linear regression. Here a standard least square algorithm was employed and the result is shown in Fig. 5 for the fourth component (80 Hz) where the straight line represents the expected value. It is important to highlight that the LSCE can not be applied when the time interval is too short; thus, it is not possible to use it to produce a graph similar to that of Fig. 5.

As a final step, increasing levels of white noise were added to the original synthetic signal. To evaluate the effect of noise, the procedure was repeated several times for each noise level and then the results shown in Fig. 4 were superimposed for a qualitative analysis.

As expected, regions where components had lower amplitudes were affected first. Initially the fourth component lost precision at its final stretch, between 1.4 s and 1.6 s, since its amplitude was already close to the background noise. As the noise amplitude rose, more regions showed instability but remarkably at signal-to-noise ratios higher than 4:1 results for most of the components were still reliable.

This behavior can be understood observing that the white noise energy is spread uniformly along

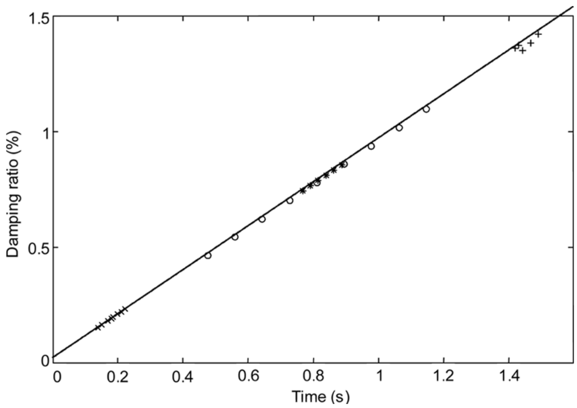

Fig. 5 Plot of calculated damping ratios over small stretches of time for the fourth component (80 Hz), showing its dependency with time. ○ - Total signal; × - Begin; + - End; ✳ - Middle

Table 3 Error (%) in the damping ratio estimation due to noise

Component	Noise Amplitude		
	5%	10%	20%
1	0.0	4.0	6.0
2	0.5	0.5	1.0
3	0.3	1.7	3.3
4	0.8	2.8	7.6

the time-frequency distribution. Thus, each point on the normalized amplitude plot receives only a small contribution of the added noise, while most of the modal energy remains concentrated. Eventually the increasing noise level would overpower the signal energy but the test showed that the statistical nature of the method allows the retrieval of reliable values even under very high signal-to-noise ratios. In order to verify this point it was performed a parametric analysis adding noise to signal. For this analysis the RMS amplitude of the noise was increased from 5% to 20% of the RMS of the original signal. The estimative of natural frequency in all cases presents less than 1% error. The errors obtained for damping ratios shown in Table 3. in general are smaller than 5% even with 20% of noise. Errors higher than 5% shown in Table 3 for the 1st and 4th components can be associated to the fact that the 1st component has the lowest amplitude of the signal and the 4th component has the damping varing with time. However it is important to mention that level of the errors for this level of the noise are acceptable in practice. These results show that the method accuracy is acceptable even in the cases for which the signal has a high level of noise.

7. Experimental setup-frame

A small structure shown in Fig. 6 was constructed in order to verify the methodology results in real cases. This model was built in stainless steel tubes with vertical bars $12.7 \times 1{,}0$ mm and horizontal bars $7{,}94 \times 0{,}07$ mm, the total weight being approximately 1,0 kg. Four accelerometers (AC1Z, AC2X, AC3X, AC4Z) were used to record data generated at four impact points during five different tests (0X, 1X, 2Z, 3Z and 4T), which were chosen to excite modes in X direction (0X and 1X), Z direction (2Z and 3Z) and torsion modes (4T). In order to record the data it was used an acquisition system with 16 bits of resolution and the response was obtained using sampling frequency equal to 200 Hz.

Table 4 presents a comparison between the results for natural frequencies obtained employing the usual procedure of Fourier transform, which corresponds to the first phase of the presented methodology, and the method LSCE. It can be observed in this table that there exists a good correlation between the two methodologies; the maximum difference between their results was 2%. Thus, the first phase of the methodology can be carried out easily, and results are accurate. It is important to recall that this phase is critical where the accuracy of the whole process is concerned, as $C_f(t, \Omega_j)$ will be computed only for the natural frequencies (Ω_j) estimated at this phase.

The function $C_f(t, \Omega_j)$ estimated for the six modes indicates linear behavior for all modes, except X1 and T1, where the damping ratio clearly changed in time.

To illustrate one case of linear behavior, Fig. 7 shows plots of the normalized curve for mode Z1,

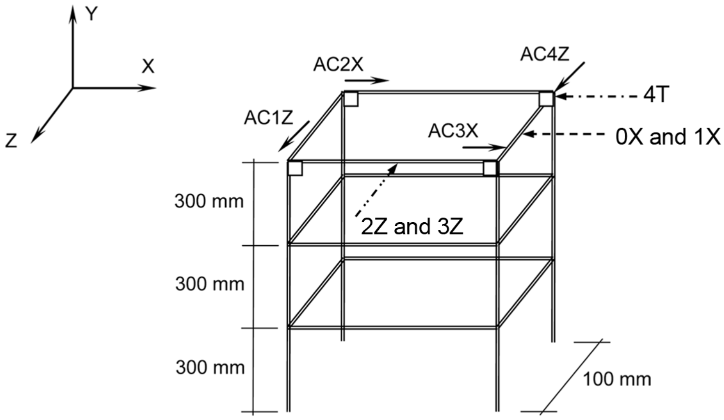

Fig. 6 Experimental setup of a space frame composed of stainless steel tubular elements with elastic modulus E = 210 GPa. Vertical bars: D = 12.70 mm, t = 1.00 mm, ρ = 40.40 g/cm^3 (where D is the external diameter, t is the thickness and ρ is the specific weight). Horizontal bars: D = 7.94 mm, t = 0.70 mm, ρ = 7.97 g/cm^3. -·-·-·-▶ - Indicates impact point (direction X) for Test 4T; ------▶ - Indicates impact point (direction X) for Tests 0X and 1X; -··-··-··▶ - Indicates impact point (direction Z) for Tests 2Z and 3Z

Table 4 Summary of results obtained experimentally through the Fourier transform and the LSCE

Mode	Fourier transform (Hz)	LSCE (Hz)
first mode of bending in X direction (X1)	15.30	15.30
first mode of bending in Z direction (Z1)	16.40	16.30
first mode of torsion (T1)	25.80	25.70
second mode of bending in X direction (X2)	53.90	53.80
second mode of bending in Z direction (Z2)	56.40	56.60
second mode of torsion (T2)	79.50	79.40

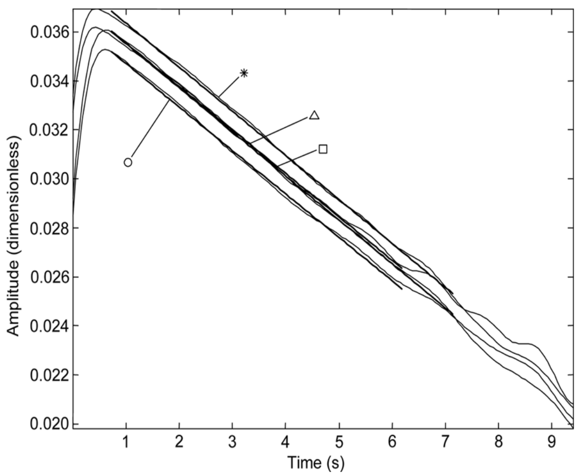

Fig. 7 Normalized amplitude plotted over time for mode Z1 (16.3 Hz). JTFD computed damping ratios ξ: ∗ - Test-3Z, AC1Z, ξ = 0.180%; △ - Test-2Z, AC1Z, ξ = 0.177%; □ - Test-3Z, AC4Z, ξ = 0.180%; ○ - Test-2Z, AC4Z, ξ = 0.177%

obtained from tests 2Z and 3Z. The damping ratio was found to be constant over all signal lifespan up to the instant 7 s, assumed to be the signal end due to the amount of oscillations. Values obtained from statistical correlation were very consistent: 0.180% for test 3Z (same value from both accelerometers) and 0.177% for test 2Z (same value from both accelerometers).

The first bending mode in the X direction presented slight nonlinearity as shown in Fig. 8 (results for test 0X) and Fig. 9 (results for test 1X). Average damping ratios were obtained for separate parts of the signal: 0.066% (3 to 11 s), 0.048% (11 to 20 s) and 0.042% (20 to 32 s).

It is important to observe the high repeatability of the damping ratios among these two tests (0X and 1X) and among signals captures from different accelerometers, AC2X and AC3X. All results

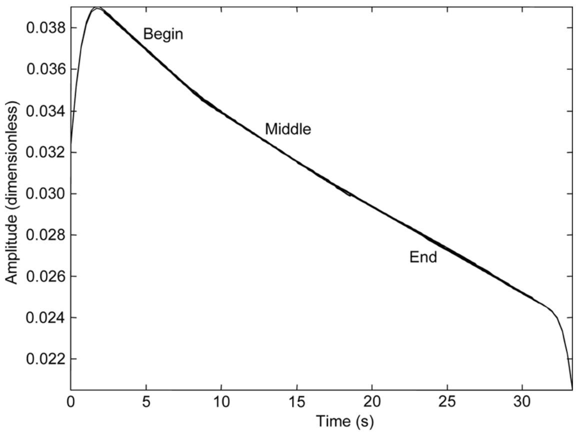

Fig. 8 Normalized amplitudes versus time for mode X1 (15.3 Hz) for test 0X. Begin: AC2X gives $\xi = 0.066\%$; AC3X gives $\xi = 0.065\%$. Middle: AC2X gives $\xi = 0.048\%$; AC3X gives $\xi = 0.047\%$. End: AC2X and AC3X give $\xi = 0.042\%$

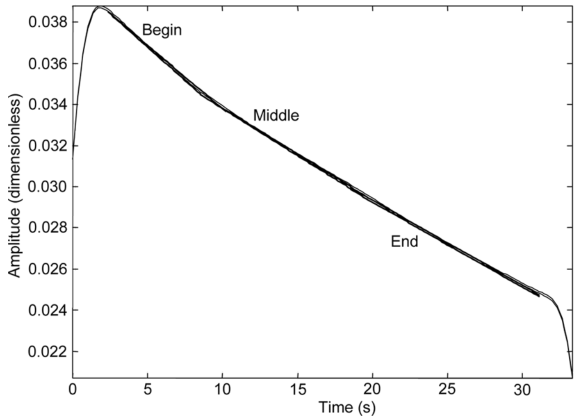

Fig. 9 Normalized amplitudes versus time for mode X1 (15.3 Hz) for test 1X. Begin: AC2X gives $\xi = 0.062\%$; AC3X gives $\xi = 0.065\%$. Middle: AC2X gives $\xi = 0.045\%$; AC3X gives $\xi = 0.046\%$. End: AC2X and AC3X give $\xi = 0.041\%$

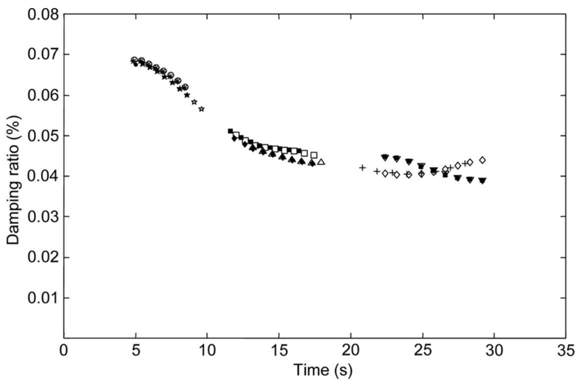

Fig. 10 Damping ratios obtained by automated slicing of the normalized amplitude graph, mode X1 (15.3 Hz). ○ - Test-0X AC2X (begin); × - Test-0X AC2X (middle); + - Test-0X AC2X (end); ✳ - Test-0X AC3X (begin); □ - Test-0X AC3X (middle); ◇ - Test-0X AC3X (end); ▽ - Test-1X AC2X (end); △ - Test-1X AC2X (middle); ☆ - Test-1X AC2X (begin); ● - Test-1X AC3X (begin); ◆ - Test-1X AC3X (middle); ■ - Test-1X AC3X (end)

showed correlation up to the third decimal digit (in %).

To highlight the repeatability of the method, all signals were divided into small stretches of time, and then linear regression was carried out to extract damping ratios. These results are depicted in Fig. 10.

Fig. 10 shows that the damping ratio starts high at 0.07% and rapidly decays to 0.045% at 15 s and then nearly remains constant assuming the value of 0.042% at 30 s. This behavior indicates the damping ratio dependence with different factors, one of them being probably the amplitude of the movement, once the displacement amplitude decays as time elapses, when the structure is in free vibration.

Table 5 presents a summary of all damping ratios obtained for each one of the six modes analised. For modes that presented non-constant damping ratios the test result was subdivided into smaller

Table 5 Condensed results (damping ratios) for all tests

Mode	Freq. (Hz)	Test	Acc	LSCE (%)	JTFD (%)		
				3-32 s	3-11 s	11-20 s	20-32 s
first mode of bending in X direction (X1)	15.30	0X	AC2X	0.05	0.066	0.048	0.042
			AC3X		0.065	0.047	0.042
		1X	AC2X		0.062	0.045	0.041
			AC3X		0.065	0.046	0.041
first mode of bending in Z direction (Z1)	16.40	2Z	AC1Z	0.17		0.177	
			AC4Z			0.178	
		3Z	AC1Z			0.181	
			AC4Z			0.180	
				1-10 s	1-4 s		4-10 s
first mode of torsion (T1)	25.80	4T	AC1Z	0.08	0.089		0.063
			AC2X		0.092		0.064
			AC3X		0.092		0.065
			AC4Z		0.092		0.065
second mode of bending in X direction (X2)	53.90	0X	AC2X	0.17		0.137	
			AC3X			0.139	
		1X	AC2X			0.144	
			AC3X			0.143	
second mode of bending in Z direction (Z2)	56.40	2Z	AC1Z	0.65		0.650	
			AC4Z			0.660	
		3Z	AC1Z			0.636	
			AC4Z			0.644	
second mode of torsion (T2)	79.50	4T	AC1Z	0.15		0.148	
			AC2X			0.150	
			AC3X			0.148	
			AC4Z			0.157	

parts where the damping ratio is supposed to be approximately constant. For comparison purposes, data from tests were also analyzed using the LSCE method.

It can be initially observed in Table 5, the great repeatability of the results of the various sensors and different tests, showing the robustness of the JTFD method. Additionally, it also possible to observe the good correlation between the results obtained by the two methods, mainly for the modes which have constant damping ratios. It can be observed that LSCE results are also close to the interval average JTFD value, a conclusion corroborated by the previous example results.

8. Conclusions

The robustness of the method presented, defined in this context as insensibility to added noise, was remarkably good. This was shown with a synthetic signal when gradually adding increasing levels of noise resulted in first loosing precision on specific regions with lower amplitude, while the remainder of the signal was preserved.

The additional step of plotting normalized amplitude curves for each mode helped to understand the behavior of a system. These graphs show not only where the damping ratios are constant but where they vary and by what amount. By slicing the normalized amplitude curves it is possible to plot the evolution of damping ratios over time, for each mode.

The method presented does not allow an easy calculation of other modal parameters, amplitude and phase angle. However, its results – damping ratio values over time for each mode – may be inserted into optimization techniques such as the LSCE, reducing their search space.

This work applied joint time-frequency distributions to calculate viscous damping ratios; however, as the JTFD method is based directly on energy loss, it can be used for most existing damping models with minor or even no modifications.

The experimental setup showed a very high repeatedly of the results. Damping ratios obtained when the method was applied to signals acquired from distinct accelerometers, even in different tests, agreed up to the third decimal figure in some cases. Varying damping ratios were easily identified by the change of slope of curves of normalized amplitude versus time.

Acknowledgements

The first author would like to thank the Brazilian National Research Council (CNPq) for the financial support during this research.

References

Allemang, R.J. and Brown, D. (1987), *Experimental Modal Analysis and Dynamic Component Synthesis*, University of Cincinnati, Ohio.

Atlas, L.E., Loughlin, P.J. and Pitton, J.W. (1992), "Signal analysis with cone kernel time-frequency representations and their application to speech", *Time-Frequency Signal Analysis*, Longman Cheshire, Sydney, Australia.

Bodeux, J.B. and Golinval, J.C. (2003), "Modal identification and damage detection using data driven stochastic subspace and ARMA methods", *Mech. Syst. Signal Pr.*, **17**(1), 83-89.

Boltežar, M. and Slavič, J. (2002), "Use of the continuous wavelet transform for the identification of damping", *Proceedings of the International Conference on Structural Dynamics Modelling*, Madeira.

Boulahbal, D., Golnaraghi, M.F. and Ismail, F. (1999), "Amplitude and phase wavelets maps for the detection of cracks in geared systems", *Mech. Syst. Signal Pr.,* **13**(3), 423-436.

Bucher, H. (2001), "Methodologies for the applications of time-frequency techniques to structural dynamics and to the boundary element method", D.Sc. Thesis, Department of Civil Engineering, COPPE/Federal, University of Rio de Janeiro. (in Portuguese)

Burrus, C.S., Gopinath, R.A. and Guo, H. (1998), *Introduction to Wavelets and Wavelet Transforms*: *A Primer*, Prentice Hall, Englewood Cliffs, New Jersey.

Carmona, R.A., Hwang, W.L. and Torrésani, B. (1997), "Characterization of signals of the ridges of their wavelets transforms", *IEEE T. Signal Proces.*, **45**(10), 2586-2590.

Clough, R.W. and Penzien, J. (1993), *Dynamics of Structures*, Second Edition, McGraw-Hill, New York.

Cohen, L. (1966), "Generalize phase-space distribution functions", *J. Math.*, **7**(5), 781-786.

Cohen, L. (1976), "Quantization problem and variational principle in the phase space formulation of quantum mechanics", *J. Math. Phys.*, **17**(10), 1863-1866.

Cohen, L. (1995), *Time-Frequency Analysis*, First Edition, New Jersey, Prentice Hall.

Cohen, L. (1996), "A general approach for obtaining joint representations in signal analysis: Part I, Characteristic function operator method", *IEEE T. Signal Proces.*, **44**(5), 1080-1090.

Choi, H.I. and Williams, W.J. (1989), "Improved time frequency representation of multicomponent signals using exponential kernels", *IEEE T. Acoust. Speech Signal Proces.,* **37**(6), 862-871.

Cunningham, G.S. and Williams, J.W. (1993), "Linear high-resolution signal synthesis for time-frequency distributions", *Proceedings of the IEEE International Conference Acoustics Speech Signal Processing*, Minneapolis, **4**(4), 400-403.

Cunningham, G.S. and Williams, J.W. (1996), "Vector-valued time-frequency representations", *IEEE T. Signal Proces.*, **44**(7), 1642-1656.

Daubechies, I. (1992), *Ten Lectures on Wavelets*, SIAM – Society for Industrial and Applied Mathematics, Pennsylvania.

Daubechies, I. (1996), "Where do wavelets come from? – A personal point of view", *Proceedings of the IEEE Special Issue on Wavelets*, **84**(4), 510-513.

Farge, M. (1992), "Wavelet transforms and their applications to turbulence", *Annu. Rev. Fluid Mech.*, **24**, 395-457.

Gökda, H. and Kopmaz, O. (2010) "A new structural damage detection index based on analyzing vibration modes by the wavelet transform", *Struct. Eng. Mech.*, **35**(2), 257-260.

Gurley, K. and Kareem, A. (1999), "Applications of wavelet transforms in wind", *Earthq. Ocean Eng., Eng. Struct.,* **21**(2), 149-167.

Gurley, K., Kijewski, T. and Kareem, A. (2003), "First - and higher-order correlation detection using wavelet transforms", *J. Eng. Mech.*, **129**(2), 188-201.

Ibrahim, S.R. and Mickulcik, E. (1977), "A method for the direct identification of vibration parameters from the free responses", *Shock Vib*., **47**(4), 183-198.

Kareem, A. and Gurley, K. (1996), "Damping in structures: its evaluation and treatment of uncertainty", *J. Wind Eng. Ind. Aerod.,* **59**(2-3), 131-157.

Kareem, A. and Kijewski, T. (2002), "Time-frequency analysis of wind effects on structures", *J. Wind Eng. Ind. Aerod.,* **90**(12-15), 1435-1452.

Katkhuda, H.N., Dwairi, H.M. and Shatarat, N. (2010), "System identification of steel framed structures with semi-rigid connections", *Struct. Eng. Mech.*, **34**(3), 351-366.

Kijewski, T. and Kareem, A. (2002a), "On the reliability of a class of system identification techniques: Insights from bootstrap theory", *Struct. Saf.*, **24**(2-4), 261-280.

Kijewski, T. and Kareem, A. (2002b), "On the presence of end effects and associated remedies for wavelet-based analysis", *J. Sound Vib.,* **256**(5), 980-988.

Kijewski, T. and Kareem, A. (2003), "Wavelet transforms for system identification in civil engineering", *Comput. Aid Civil Infrast. Eng.*, **18**(5), 339-355.

Lamarque, C.H., Pernot, S. and Cuer, A. (2000), "Damping identification in multi-degree-of-freedom systems via a wavelet-logarithmic decrement – Part 1: Theory", *J. Sound Vib.,* **253**(3), 361-374.

Lin, J. and Qu, L. (2000), "Feature extraction based on morlet wavelet and its application for mechanical fault diagnosis", *J. Sound Vib.,* **234**(1), 135-148.

Magluta, C., Roitman, N., Viero, P.F. and Rosa, L.F.L. (2001), "Experimental estimation of physical properties of a flexible riser", XX OMAE – *International Conference on Offshore Mechanics and Arctic Engineering*, Rio de Janeiro.

Mohanty, P. and Rixen, D.J. (2006), "Modified ERA method for operational modal analysis in the presence of harmonic excitations", *Mech. Syst. Signal Pr.*, **20**, 114-130.

Mallat, S. (1999), *A Wavelet Tour of Signal Processing*, Academic Press, New York.

Meirovich, L. (1986), *Elements of Vibration Analysis*, McGraw-Hill, New York.

Morlet, J., Arens, G., Fourgeau, E. and Giard, D. (1982), "Wave propagation and sampling theory", *Geophysics*, **47**(2), 203-236.

Nagarajaiah, S. and Basu, B. (2009), "Output only modal identifi cation and structural damage detection using time frequency & wavelet techniques", *Earthq. Eng. Eng. Vib.*, **8**(4), 583-605.

Paz, M. and Leigh, W. (2003), *Structural Dynamics. Theory and Computation*, Fifth Edition, Kluwer Academic Publisher, Massachusetts.

Peters, D.R. (2005), *Mesoscale Quantization and Self-Organized Stability*, http://arXiv.org/abs/physics/0506143.

Piombo, B.A.D., Fasana, A., Marchesiello, S. and Ruzzene, M. (2000), "Modelling and identification of the dynamic response of a supported bridge", *Mech. Syst. Signal Proces.*, **14**(1), 74-89.

Rao, S.S. (1995), *Mechanical Vibrations*, Third Edition, Addison-Wesley, Reading.

Rioul, O. and Duhamel, P. (1992), "Fast algorithms for discrete and continuous wavelet transforms", *IEEE T. Inform. Theory,* **38**(2), 569-586.

Roshan-Ghias, A., Shamsollahi, M.B., Mobed, M. and Behzad, M. (2007), "Estimation of modal parameters using bilinear joint time-frequency distributions", *Mech. Syst. Signal Proces.,* **21**, 2125-2136.

Staszewski, W.J. and Tomlinson, G.R (1994), "Application of the wavelet transform to fault detection in a spur gear", *Mech. Syst. Signal Proces.,* **8**(3), 289-307.

Staszewski, W.J. (1997), "Identification of damping in MDOF systems using time-scale decomposition", *J. Sound Vib.,* **203**(2), 283-305.

Staszewski, W.J. (1998), "Identification of non-linear systems using multi-scale ridges and skeletons of the wavelet transform", *J. Sound Vib.,* **214**(4), 639-658.

Todorovska, M.I. (2001), "Estimation of instantaneous frequency of signals using the continuous wavelet transform", Report CE 01-07, Department of Civil Engineering, University of Southern California.

Thomson, W.T. and Dahleh, M.D. (1998), *Theory of Vibration*, Prentice Hall, New Jersey.

Ville, J. (1946), "Theory and applications of the concept of analytic signal", *Cable. Trans.,* **2**(1), 61-74. (in French)

Wang, S. and Liu, F. (2010), "New accuracy indicator to quantify the true and false modes for eigensystem realization algorithm", *Struct. Eng. Mech.*, **34**(5), 625-634.

Weaver, Jr., W. and Jonhnston, P.R. (1987), *Structural Dynamics by Finite Elements*, Prentice Hall, Englewood Cliffs, New Jersey.

Wigner, E.P. (1932), "On the quantum correction for thermodynamic equilibrium", *Phys. Rev.*, **40**, 749-759.

Wigner, E.P. (1971), "Quantum-mechanical distribution functions revisited, in W. Yourgrau and Van der Merwe", *Perspectives in Quantum Theory*, MIT Press.

Zhang, Y., Zhang, Z., Xu, X. and Hua, H. (2005), "Modal parameter identification using response data only", *J. Sound Vib.*, **282**, 367-380.

Zhao, Y., Atlas, L.E. and Marks, R.J. (1990), "The use of cone-shaped kernels for generalized time-frequency representations of nonstationary signals", *IEEE T. Acoust. Speech Signal Proc.,* **38**(7), 1084-1091.